J. Wind Eng. Ind. Aerodyn. 133 (2014) 92–100

Contents lists available at ScienceDirect

Journal of Wind Engineering and Industrial Aerodynamics

journal homepage: www.elsevier.com/locate/jweia

Wind spectrum and correlation characteristics relative to vehicles moving through cross wind field

Mengxue Wu [a], Yongle Li [a,*], Xinzhong Chen [b], Peng Hu [a]

[a] Department of Bridge Engineering, Southwest Jiaotong University, 610031 Chengdu, Sichuan, PR China
[b] Wind Science and Engineering Research Center, Department of Civil and Environmental Engineering, Texas Tech University, Lubbock, Texas 79409-1023, USA

ARTICLE INFO

Article history:
Received 10 March 2014
Received in revised form
7 August 2014
Accepted 7 August 2014
Available online 28 August 2014

Keywords:
Wind spectrum
Correlation characteristics
Coherence function
Moving vehicles
Taylor's frozen turbulence hypothesis
Isotropic turbulence model

ABSTRACT

In this study, based on Taylor's frozen turbulence hypothesis and isotropic turbulence model, the auto-correlation coefficient function of lateral wind fluctuation and cross-correlation coefficient functions of lateral and longitudinal wind fluctuations are derived from the Kaimal spectrum of longitudinal wind fluctuation. Based on the same hypothesis, this study also derived formulations for calculating the power spectra and correlation coefficient functions of wind turbulence relative to moving vehicles. The results can be applied for any vehicle moving direction, and for both longitudinal and lateral components of wind turbulence. The effects of speed ratio of moving vehicle to mean wind velocity and vehicle direction on the characteristics of wind turbulence relative to moving vehicles are investigated. In addition, a closed-form expression is also proposed to approximately represent the square-root coherence function of wind turbulence relative to moving vehicles. It provides useful insights for better understanding the characteristics of turbulent wind relative to moving vehicles, and also provides a theoretical foundation for solving the discontinuity of sudden change of wind fluctuations while the wind fluctuations are simulated using traditional fixed-point spectrum.

1. Introduction

The safety and comfort of running vehicles in strong crosswind conditions become one of increasingly important issues needing to be addressed as vehicle operating speed increases and weight decreases (Baker, 1991a, 1991b, 1991c, 2013; Diedrichs, 2006; Gawthorpe, 1994; Johnson, 1996). Currently, time domain simulation frameworks are often used to quantify dynamic response of running vehicles in crosswind conditions. The time histories of random wind velocity fluctuations at finite discrete fixed-locations are generated with prescribed spectral characteristics (Cai and Chen, 2004; Li et al., 2005; Xu and Guo, 2003). The wind fluctuations on the running vehicles are then approximately estimated from these wind fluctuations using some kind of spatial extrapolation scheme (e.g., Liu, 2011), or simply taking the values at the nearest fixed-locations. These approximate modeling of wind fluctuations on vehicles often causes discontinuity and may even introduce sudden changes in the wind fluctuations, which is clearly inconsistent with the actual situation. As a result, the corresponding aerodynamic forces on vehicles and the estimated vehicle dynamic response, especially, the peak response, are noticeably affected. The estimations with this type of modeling of wind fluctuations may not well represent the actual performance of vehicles in crosswind conditions. This is particularly true in cases when wind speed and/or vehicle speed are high.

In order to more accurately and also more effectively model wind fluctuations on running vehicles, a random process model for atmospheric turbulence seen from a running vehicle is required. This modeling also facilitates calculation of the aerodynamic forces and dynamic response of moving vehicles in frequency domain by spectral analysis. Balzer (1977) discussed the effect of atmospheric turbulence on moving vehicles and derived the power spectral density (PSD) function of turbulence encountered by a high-speed ground transport vehicle, where the contribution of crosswind component of wind fluctuation was neglected. Cooper (1984) calculated the PSD, cross-correlation and coherence of wind fluctuations normal to a moving vehicle using von Karman spectrum for wind turbulence at fixed-locations. Based on the wind characteristics with respect to a moving vehicle derived in Cooper (1984), Baker (1991b and 1991c) presented a comprehensive study on unsteady aerodynamic forces and dynamic response of vehicles in frequency, amplitude and time domains. A more comprehensive framework was proposed in Baker (2013) for the consideration of the effects of crosswinds on trains, which can be applied in the train authorization and route risk analysis.

In present study, based on Taylor's frozen turbulence hypothesis and isotropic turbulence model, the auto-correlation

* Corresponding author. Tel.: +86 13540001365.
E-mail addresses: lele@swjtu.edu.cn, ceyongle@gmail.com (Y. Li).

http://dx.doi.org/10.1016/j.jweia.2014.08.004
0167-6105/

coefficient function of lateral wind fluctuation and cross-correlation coefficient functions of lateral and longitudinal wind fluctuations are derived from the Kaimal spectrum of longitudinal wind fluctuation. The power spectra and correlation coefficient functions of wind turbulence relative to moving vehicles are also deduced based on the same hypothesis. The results can be applied for any vehicle moving direction, and for both longitudinal and lateral components of wind turbulence. The effects of speed ratio of moving vehicle to mean wind velocity and vehicle direction on the characteristics of wind turbulence relative to moving vehicles are investigated. A closed-form expression is also proposed to approximately represent the square-root coherence function of wind turbulence relative to moving vehicles.

2. Turbulence characteristics at fixed points

2.1. Power spectrum of longitudinal turbulence

In this study, it is defined that the mean wind velocity $U(z)=\overline{U}$ at the height z above the ground is along the x-axis, and u, v and w are the instantaneous longitudinal, lateral and vertical components of fluctuating wind velocities along the x-, y- and z-axes, respectively, as shown in Fig. 1. In the following analysis, only the u- and v-components of wind fluctuations are discussed as they are relevant to vehicle aerodynamics. The PSD of u-component, $S_u(n)$, is given as the Kaimal spectrum (Kaimal et al., 1972):

$$\frac{nS_u(n)}{u_*^2}=\frac{200\hat{n}}{(1+50\hat{n})^{5/3}} \tag{1}$$

where n is the frequency in Hz; $\hat{n}=nz/\overline{U}$ is the non-dimensional frequency; u_* is the shear velocity of the flow. The standard deviation (STD) of u-component is then given as $\sigma_u=\sqrt{6}u_*$.

2.2. Taylor's frozen turbulence hypothesis and isotropic turbulence assumption

Taylor's frozen turbulence hypothesis originated in the paper (Taylor, 1938) which mainly discussed the connection between the spectrum of turbulence at a fixed point and the correlation between simultaneous values of velocity at two points. It is postulated that if the mean wind speed is sufficiently high, the flow pattern of the turbulence field then does not have time to change, and passes a fixed point with the mean wind speed. The sequence of changes in fluctuation at the fixed point is simply due to the passage of an unchanging pattern of turbulent motion over the point. Furthermore, it's worth noting that Taylor's hypothesis has been verified by wind tunnel tests conducted by Mr L.F.G. Simmons (Taylor, 1938). Based on this hypothesis, the wind fluctuations at two points along the mean wind speed direction

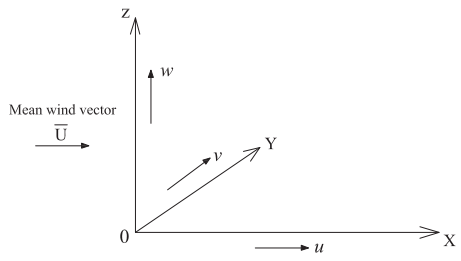

Fig. 1. The mean wind vector and three components of fluctuating velocities, (symbol: u=longitudinal component of fluctuating wind velocity; v=lateral component of fluctuating wind velocity; w=vertical component of fluctuating wind velocity).

are related as follows:

$$u(x,t)=u(x-\overline{U}t,0),\ v(x,t)=v(x-\overline{U}t,0) \tag{2}$$

Taylor (1938) also proved that the turbulence was in fact isotropic, as the measurements in wind tunnel tests had good agreement with those obtained from the theoretical analysis by Karman (1937). Landahl and Christensen (1992) pointed out that Taylor's hypothesis is based on the isotropic turbulence assumption, which means the isotropic turbulent coordinate system is moving along with the mean wind velocity.

Some studies (Lin, 1953; Gifford, 1956; Lappe and Davidson, 1963) proved that Taylor's frozen turbulence hypothesis had a validity range. Both the investigations from Lin (1953) and Gifford (1956) indicated that there was a range where Taylor's hypothesis was certainly valid for atmospheric motions and that this region was generally in the high frequency portion of the spectrum. Furthermore, a unique tower-airplane experiment was conducted by Lappe and Davidson (1963), which permitted a comparison between airplane and concurrent tower measurements of atmospheric turbulence. It indicated that the Taylor's hypothesis was approximately correct for wavelength $(\overline{U}/n)$ less than about 300 m. If the mean wind velocity $\overline{U}=30$ m/s, then the Taylor's hypothesis is valid for the frequency range $n>0.1$ Hz. The significant frequency range for ground vehicles is above 0.1 Hz. Thus, it is valid for engineering application that Taylor's frozen turbulence hypothesis can be applied to study the unsteady aerodynamics of moving vehicles.

Admittedly, both the Taylor's frozen turbulence hypothesis and isotropic turbulence assumption are not strictly true and involve certain approximation of the real atmospheric wind filed. However, as discussed above, for our research purpose and the concerned frequency range, both the Taylor's hypothesis and isotropic turbulence assumption are approximately correct, and the resulted observations are useful in practical engineering application.

For the moving vehicle submerged in the actual turbulence, there indeed exists interaction between the surface of the vehicle and the around wind flow field. This aerodynamic interaction between vehicle and the around wind field is actually reflected by aerodynamic coefficients including aerodynamic admittance, which can be determined in wind tunnel or from CFD simulation under given turbulent wind field. The study on aerodynamics coefficients is beyond the scope of this study.

2.3. Auto-correlation coefficient functions of turbulence

Auto-correlation and power spectral density functions are Fourier transform pair. The auto-correlation coefficient function at a stationary point can be obtained from the Kaimal longitudinal spectrum by Fourier transformation as shown in Eq. (3):

$$\begin{aligned}\rho_u(\tau)&=\frac{1}{\sigma_u^2}\int_0^{+\infty}S_u(n)\cos(2\pi n\tau)dn\\&=1-0.036\tilde{r}^2+0.2\tilde{r}^{7/6}LommelS2\left(\frac{11}{6},\frac{1}{2},\frac{\pi}{25}\tilde{r}\right)\end{aligned} \tag{3}$$

where $\tilde{r}=\tau\overline{U}/z$ is a non-dimensional variable; and $LommelS2$ (p,q,x) is a special function with three parameters, which is the second kind of solutions of equation $x^2y''+xy'+(x^2-q^2)y=x^{p+1}$ (Gradsbteyn and Ryzbik, 2000).

For the convenience of subsequent calculations, Eq. (3) is numerically fitted as the following formulation of non-dimensional variable $\tilde{r}$, i.e., $\rho_u(\tau)=f(\tilde{r})$. As shown in Fig. 2, both are almost identical.

$$\begin{aligned}f(\tilde{r})=&0.013+0.467\exp(-\tilde{r}/4.296)+0.201\exp(-\tilde{r}/0.797)\\&+0.281\exp(-\tilde{r}/15.742)\end{aligned} \tag{4}$$

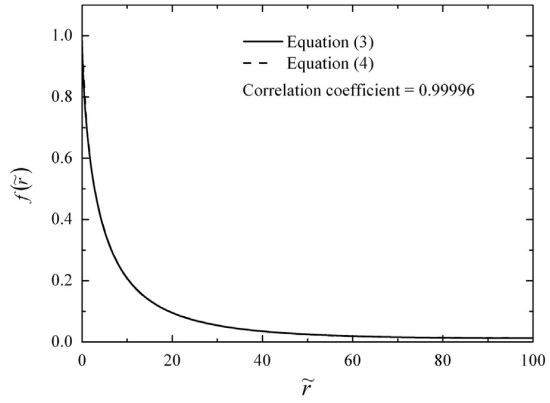

Fig. 2. The fitting curve of longitudinal auto-correlation coefficient function, (abscissa: $\tilde{r}$=non-dimensional variable; ordinate: $f(\tilde{r})$=longitudinal auto-correlation coefficient function).

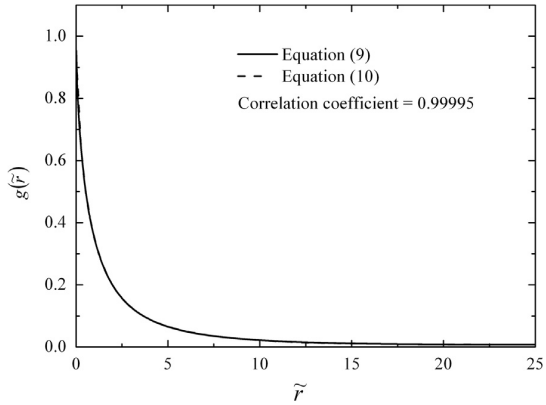

Fig. 4. The fitting curve of lateral auto-correlation coefficient function, (abscissa: $\tilde{r}$=non-dimensional variable; ordinate: $g(\tilde{r})$=lateral auto-correlation coefficient function).

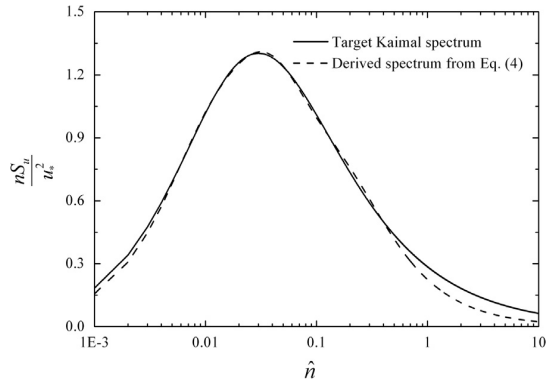

Fig. 3. The comparison of target Kaimal spectrum and derived spectrum, (abscissa: $\hat{n}$=non-dimensional frequency; ordinate: nS_u/u_*^2=reduced power spectral density).

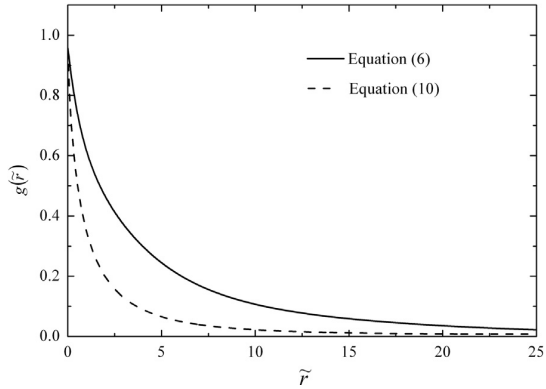

Fig. 5. The comparison of lateral auto-correlation coefficient functions, (abscissa: $\tilde{r}$= non-dimensional variable; ordinate: $g(\tilde{r})$= lateral auto-correlation coefficient function).

The power spectral density function can also be obtained from the auto-correlation coefficient function represented by Eq. (4) with Fourier transformation. The target Kaimal spectrum and the derived spectrum from Eq. (4) for the longitudinal u-component are compared in Fig. 3. It can be observed from this figure that the derived spectrum nearly coincides with the target Kaimal spectrum, except that there is a slight deviation at high frequencies (>1 Hz), which is due to the differences caused by the longitudinal auto-correlation coefficient functions, given by Eqs. (3) and (4). The approximation is considered to be acceptable for engineering applications.

The auto-correlation coefficient function of lateral wind fluctuation, i.e., $\rho_v(\tau)=g(\tilde{r})$ can be obtained from the longitudinal auto-correlation coefficient function $\rho_u(\tau)=f(\tilde{r})$ under the assumption of isotropic turbulence (ESDU, 1985):

$$g(\tilde{r})=f(\tilde{r})+\frac{1}{2}\Delta r\frac{df(\tilde{r})}{d(\Delta r)} \tag{5}$$

where $\Delta r=\tau\overline{U}$.

Substituting Eq. (4) into Eq. (5), the lateral auto-correlation coefficient function $g(\tilde{r})$ can be expressed as

$$\begin{aligned} g(\tilde{r}) &= 0.013+(0.467-0.054\tilde{r})\exp(-\tilde{r}/4.296)\\ &\quad +(0.201-0.126\tilde{r})\exp(-\tilde{r}/0.797)\\ &\quad +(0.281-0.009\tilde{r})\exp(-\tilde{r}/15.742) \end{aligned} \tag{6}$$

Other than the above method based on the isotropic assumption, the lateral auto-correlation coefficient function $g(\tilde{r})$ can also be directly calculated from the PSD of v-component, $S_v(n)$, when it is available. The spectrum of v-component, $S_v(n)$, is given as follows (Kaimal et al., 1972):

$$\frac{nS_v(n)}{u_*^2}=\frac{15\hat{n}}{(1+9.5\hat{n})^{5/3}} \tag{7}$$

The standard deviation σ_v of v-component can be able to be derived from Eq. (7):

$$\sigma_v^2=\int_0^{+\infty}S_v(n)dn=2.368u_*^2 \tag{8}$$

then $\sigma_v/\sigma_u\approx 0.628$.

It leads to

$$\begin{aligned} g(\tilde{r}) &= \frac{1}{\sigma_v^2}\int_0^{+\infty}S_v(n)\cos(2\pi n\tau)dn\\ &= 1-0.984\tilde{r}^2+1.389\tilde{r}^{7/6}LommelS2\left(\frac{11}{6},\frac{1}{2},\frac{4\pi}{19}\tilde{r}\right) \end{aligned} \tag{9}$$

and can be further approximated as follows, which gives almost identical results as shown in Fig. 4.

$$\begin{aligned} g(\tilde{r}) &= 0.008+0.224\exp(-\tilde{r}/3.579)\\ &\quad +0.485\exp(-\tilde{r}/0.966)+0.235\exp(-\tilde{r}/0.190) \end{aligned} \tag{10}$$

The comparison of lateral auto-correlation coefficient functions calculated from Eqs. (6) and (10) is shown in Fig. 5. It is observed that the decay rate of lateral auto-correlation coefficient function represented by Eq. (10) is greater than that of Eq. (6). In other

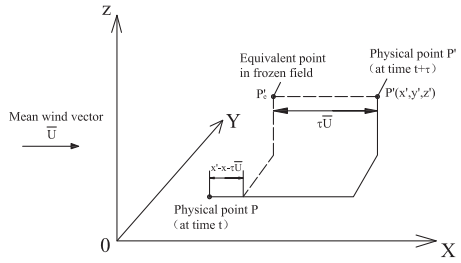

Fig. 6. Geometry of physical and equivalent points in a frozen turbulence field (Cooper, 1984).

words, the isotropic assumption results in the stronger lateral auto-correlation at a fixed point in space and the lateral fluctuating load at this point is more conservative. In present study, the isotropic assumption is adopted because of the more conservative lateral auto-correlation coefficient function and more simple derivation process. The use of isotropic turbulence assumption permits the turbulence characteristics defined completely by the longitudinal turbulence PSD, which is given in Kaimal spectrum.

2.4. Cross-correlation coefficient functions of turbulence

Consider the cross-correlation of turbulence at two fixed points at space P and P'. The position vectors of P and P' are $\vec{r}(x,y,z)$ and $\vec{r'}(x',y',z')$, respectively. Consider the cross-correlation coefficient function of the turbulence at the two points with a time lag of τ. Invoking Taylor's hypothesis, the time lag τ can be related to an equivalent spatial separations $\tau\overline{U}$ in the negative direction of the mean wind speed. Thus, referring to Fig. 6, there is an equivalent point $P_{e'}$ in the frozen field (frozen at time t) corresponding to the physical point P'. The equivalent separations between points P and $P_{e'}$ along the x, y and z axes in the frozen field are:

$$\Delta x_e = x' - x - \tau\overline{U} \tag{11}$$

$$\Delta y = y' - y \tag{12}$$

$$\Delta z = z' - z \tag{13}$$

Consequently, the turbulence cross-correlation at two points P and P' is equivalent to the spatial cross-correlation at two points P and P_e' in the frozen field. Under the assumption of isotropic turbulence, the cross-correlation coefficient function is expressed as (Batchelor, 1953; Cooper, 1984; ESDU, 1986):

$$\rho_{ij}(\vec{r},\vec{r'};\tau) = c_{ij}f(\tilde{r}) + (1-c_{ij})g(\tilde{r}) \tag{14}$$

where $f(\tilde{r})$ and $g(\tilde{r})$ are the longitudinal and lateral auto-correlation coefficient functions, respectively; $\overline{U}$ is the average of the mean wind speed at points P and P', approximately $\overline{U} = \overline{U}_{Z_m}$, $z_m = \frac{1}{2}(z+z')$; $\tilde{r} = \Delta r_e/z_m$, $\Delta r_e = \sqrt{\Delta x_e^2 + \Delta y^2 + \Delta z^2}$; for $i,j = u$, $c_{uu} = (\Delta x_e/\Delta r_e)^2$; for $i,j = v$, $c_{vv} = (\Delta y/\Delta r_e)^2$; for $i = u, j = v$, $c_{uv} = \Delta x_e \Delta y/\Delta r_e^2$.

Fig. 7 displays the cross-correlation coefficient functions of u-component, v-component, and between u- and v-components of points P and P'. It is assumed that the non-dimensional separation between physical points P and P' along the x, y and z axes are: $\tilde{d}_x = (x'-x)/z_m = 0.5$, $\tilde{d}_y = (y'-y)/z_m = 0.5$, $\tilde{d}_z = (z'-z)/z_m = 0$, and the non-dimensional time lag is defined as $\tilde{\tau} = \tau\overline{U}/z_m$. It is observed that the cross-correlation of u-component is stronger than those of v-component, and between u- and v-components. The cross-correlation between u- and v-components is often considered to be negligibly small. However, the result in Fig. 7 indicates that the cross-correlation between u- and v-components is noticeable in isotropic turbulence.

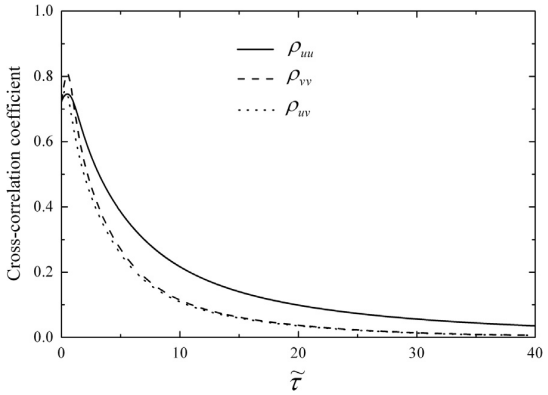

Fig. 7. The cross-correlation coefficient functions between two stationary points, (abscissa: $\tilde{\tau}$ = non-dimensional time lag; symbol: ρ_{uu} = cross-correlation coefficient function of u-component; ρ_{vv} = cross-correlation coefficient function of v-component; ρ_{uv} = cross-correlation coefficient function between u- and v-components).

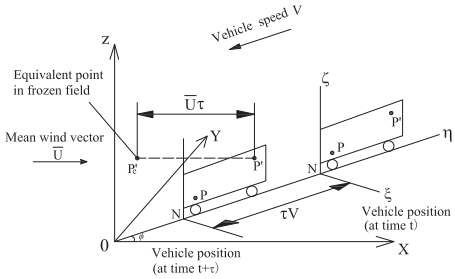

Fig. 8. Geometry of two points moving with the vehicle and equivalent point (Cooper, 1984).

3. Turbulence characteristics relative to moving vehicle

3.1. Cross-correlation coefficient functions of turbulence

Referring to Fig. 8, a vehicle is moving at a constant speed V along a straight line N–0 through the origin of the global coordinate system 0–XYZ, at an angle φ to the X-axis. The global coordinate system 0–XYZ is fixed on the earth. The local coordinate system N–$\xi\eta\zeta$ (origin N) is fixed on the vehicle, with the plane N-η-ζ is close to the surface of the vehicle. The two physical points P and P' are fixed on the moving vehicle, and the local coordinates of P and P' are $(0,\eta,\zeta)$ and $(0,\eta',\zeta')$, respectively. The vehicle is moving from one position at time t to another at time $t+\tau$. Then the position vectors $\vec{r}(t)$ of P and $\vec{r}'(t+\tau)$ of P' in the global coordinate system can be found. The question is to determine the turbulence cross-correlation at points P and P' with time delay τ. Applying Taylor's frozen turbulence hypothesis, an equivalent point P_e' in the frozen turbulence field (at time t) can be found corresponding to the physical point P' (at time $t+\tau$), which is a distance $\tau\overline{U}$ away from point P' in the negative X-axis. Thus, the turbulence cross-correlation at two points P and P' fixed in the moving vehicle is equivalent to the spatial cross-correlation at two points P and P_e' in the frozen field. The equivalent separations between points P and P_e' along the X, Y and Z axes in the frozen field are given as Eqs. (15)–(17). Thus the wind characteristics relative to a moving vehicle could be described in the global

coordinate system 0–*XYZ* fixed on the earth.

$$\Delta x_e = (\eta' - \eta - V\tau)\cos\ \varphi - \tau\overline{U} \tag{15}$$

$$\Delta y_e = (\eta' - \eta - V\tau)\sin\ \varphi \tag{16}$$

$$\Delta z = \zeta' - \zeta \tag{17}$$

The expression form of the turbulence cross-correlation coefficient function relative to moving vehicles is identical to the cross-correlation in the fixed coordinate system (Cooper, 1984). Compared to the stationary points, the only change is the equivalent separations between the two points fixed in the moving vehicle. Referring to Eq. (14), it can be expressed as:

$$\rho_{ij}^{M}(\overrightarrow{r}, \overrightarrow{r}'; \tau) = c_{ij} f(\tilde{r}) + (1 - c_{ij}) g(\tilde{r}) \tag{18}$$

where the superscript M represents that the vehicle motion is considered; $f(\tilde{r})$ and $g(\tilde{r})$ are the longitudinal and lateral auto-correlation coefficient functions, respectively; $\tilde{r} = \Delta r_e / z_m$; $\Delta r_e = \sqrt{\Delta x_e^2 + \Delta y_e^2 + \Delta z^2}$; $z_m = \frac{1}{2}(z + z')$; for $i,j = u$, $c_{uu} = (\Delta x_e / \Delta r_e)^2$; for $i,j = v$, $c_{vv} = (\Delta y_e / \Delta r_e)^2$ for $i = u, j = v$, $c_{uv} = \Delta x_e \Delta y_e / \Delta r_e^2$.

3.2. Auto-correlation coefficient functions and power spectra of turbulence

The auto-correlation coefficient function of turbulence at the moving point P can be readily obtained from Eq. (18) by setting the two points are identical, i.e., $\Delta x_e = -V\tau\ \cos\ \varphi - \tau\overline{U}$, $\Delta y_e = -V\tau\ \sin\ \varphi$, and $\Delta z = 0$. The power spectra of i-component ($i = u, v$) can be given as

$$S_i^M(n) = \sigma_i^2 \int_0^{+\infty} \rho_i^M(\tau)\cos(2\pi n\tau)d\tau = 4u_*^2 \frac{z}{V_r}\sqrt{\frac{\pi}{2}}[d_i A + (1 - d_i)(A - B - C - D)] \tag{19}$$

where for $i = u$,

$$d_u = [(\overline{U} + V\ \cos\ \varphi)/V_r]^2 \tag{20}$$

for $i = v$,

$$d_v = [(V\ \sin\ \varphi)/V_r]^2 \tag{21}$$

$$V_r = \sqrt{\overline{U}^2 + V^2 + 2\overline{U}V\ \cos\ \varphi} \tag{22}$$

$$A = \frac{0.52017}{0.05419 + s^2} + \frac{1.20867}{1.57290 + s^2} + \frac{0.08540}{0.00404 + s^2} \tag{23}$$

$$B = \frac{0.01409(1 - 18.45244s^2)}{(0.05419 + s^2)^2} \tag{24}$$

$$C = \frac{0.95056(1 - 0.63577s^2)}{(1.57290 + s^2)^2} \tag{25}$$

$$D = \frac{0.00017(1 - 247.81938s^2)}{(0.00404 + s^2)^2} \tag{26}$$

$$s = 2\pi\hat{n} \tag{27}$$

$$\hat{n} = \frac{nz}{V_r} \tag{28}$$

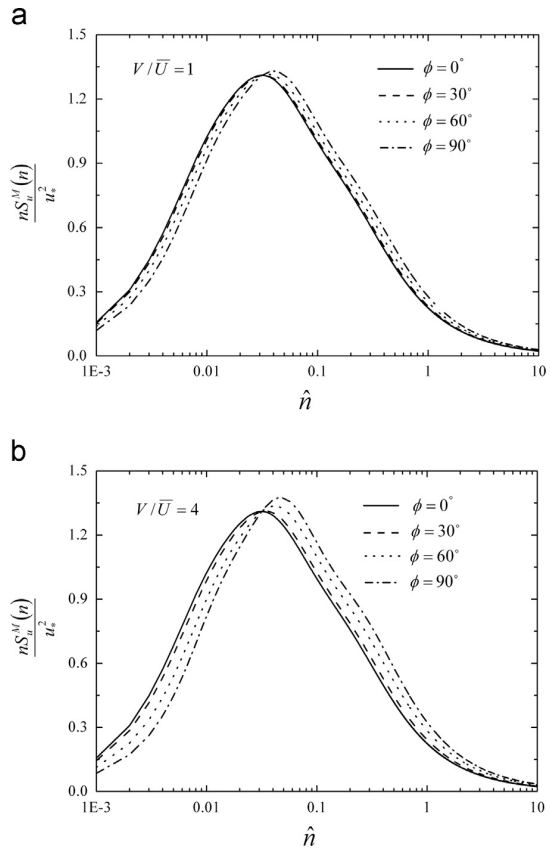

Fig. 9. The influence of angle φ on power spectrum of u-component: (a) $V/\overline{U} = 1$, (b) $V/\overline{U} = 4$, (symbol: $\varphi =$ vehicle moving direction; $V/\overline{U}$=speed ratio).

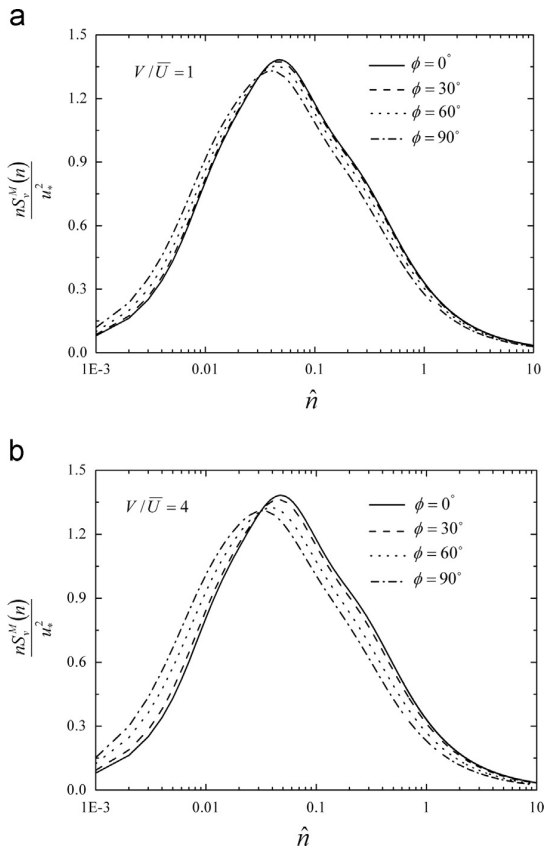

Fig. 10. The influence of angle φon power spectrum of v-component: (a) $V/\overline{U} = 1$, (b) $V/\overline{U} = 4$, (symbol: φ=vehicle moving direction; $V/\overline{U}$=speed ratio).

It can be readily illustrated that when the vehicle is stationary ($V=0$), the above wind characteristics relative to moving vehicles reduce to those at fixed points. It is also noted that the STDs of u- and v-components of turbulence relative to moving vehicle are not affected by the moving vehicle, i.e., $\sigma_u^M=\sigma_u$ and $\sigma_v^M=\sigma_v$.

When $V\ll\overline{U}$, it can be assumed to neglect the higher-order items, such as V^2 and $\overline{U}V$, then $d_u\approx 1$, $d_v\approx 0$ and $V_r\approx\overline{U}$. While $\overline{U}\ll V$, $\overline{U}^2$and $\overline{U}V$ can be ignored, then $d_u\approx\cos^2\varphi$, $d_v\approx\sin^2\varphi$, $V_r\approx V$. When the wind direction is normal to the moving vehicle (i.e., $\varphi=90^\circ$), $d_u\approx 0$, $d_v\approx 1$for $\overline{U}\ll V$.

4. Discussion on the characteristics of wind turbulence relative to moving vehicle

4.1. Wind power spectra

Figs. 9 and 10 show the influence of vehicle moving direction, i.e., the angle φ, on the power spectra of u- and v-components of wind fluctuation at a point fixed on moving vehicle, and the speed ratios $V/\overline{U}=1$ and 4. It is observed that the spectrum of u-component shifts into higher frequencies with increasing angle φ, which is more significant with increasing speed ratio. However, the influence of vehicle moving direction on the spectrum of v-component is opposite to u-component, i.e., the spectrum of v-component shifts into lower frequencies with increasing angle φ.

Fig. 11 displays the influence of speed ratio on the spectra of u- and v-components of wind fluctuation, where the wind direction is normal to the moving vehicle, i.e., $\varphi=90^\circ$. It is seen that the spectrum shifts into higher frequencies. As a result, the energy in the range 0.2-4.0 Hz increases with increasing speed ratio. This is important to a rail vehicle which has the first natural frequency range from 0.5 Hz to 1.0 Hz (Cheli et al., 2012) and has the lower modal frequencies of the suspension located in the range 0.5–5.0 Hz (Cooper, 1984). It indicates that the effect of movement is to make the moving vehicle experience higher wind energy at the frequency range of interest, thus leads to higher aerodynamic forces.

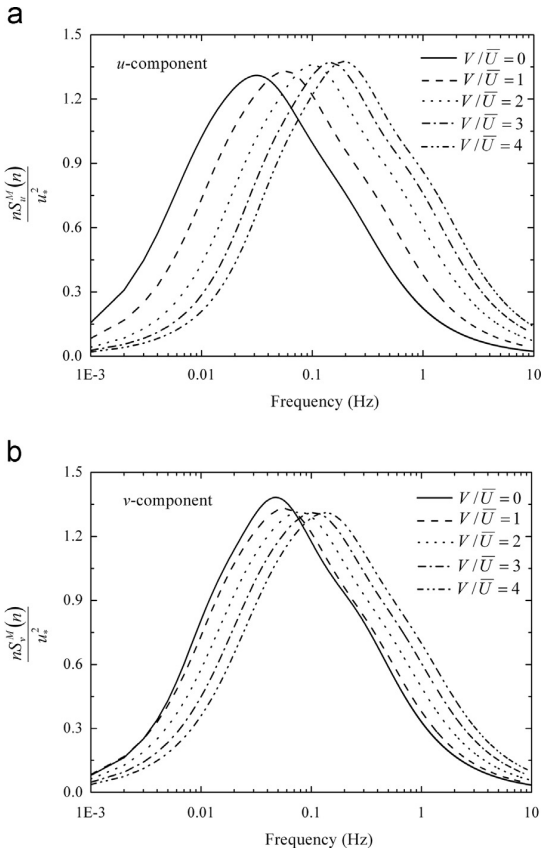

Fig. 11. The influence of speed ratio on power spectra of u- and v-components: (a) u-component; (b) v-component, (symbol: $V/\overline{U}$=speed ratio).

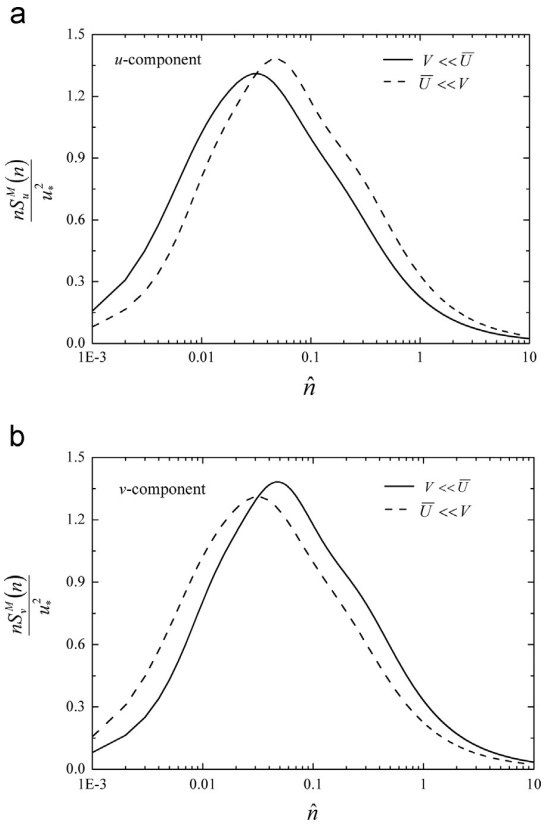

Fig. 12. Power spectra of u- and v-components under the two extreme conditions: (a) u-component; (b) v-component, (symbol: $V=$ vehicle speed; $\overline{U}=$ mean wind velocity).

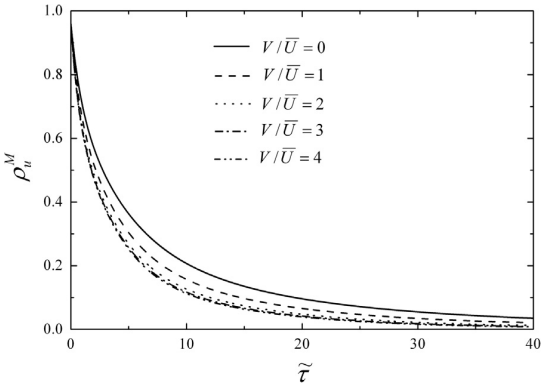

Fig. 13. The longitudinal auto-correlation coefficient function at different speed ratios, (abscissa: $\tilde{\tau}$=non-dimensional time lag; ordinate: ρ_u^M=longitudinal auto-correlation coefficient function relative to moving vehicle; symbol: $V/\overline{U}=$ speed ratio).

Fig. 12 compares the power spectra of u- and v-components of wind fluctuation at a point fixed on moving vehicle under the two extreme conditions $V \ll \overline{U}$ and $\overline{U} \ll V$, where the wind direction is normal to the moving vehicle, i.e., $\varphi = 90^\circ$. Compared with the condition of $V \ll \overline{U}$, it is seen that the spectrum of u-component shifts into higher frequencies under the condition of $\overline{U} \ll V$. But on the contrary, the spectrum of v-component shifts into lower frequencies.

4.2. Auto-correlation coefficient function and turbulence length scale

Fig. 13 displays the longitudinal auto-correlation coefficient function at different speed ratios where$\varphi = 90^\circ$. The normalized non-dimensional time variable is defined as $\tilde{\tau} = \tau V_r / z$. The integrations of these auto-correlation coefficients give the corresponding turbulence length scale. It is observed that the length scale 'seen' from the moving vehicle decreases with increasing speed ratio. It indicates that compared with the stationary case, the motion of vehicle results in reducing the time of vehicle passing by the turbulent eddies, corresponding to the reduction of the average size of turbulent eddies 'seen' from the moving vehicle. In addition, it should be noted that the sensitivity of the auto-correlation coefficient function to the speed ratio reduces with increasing speed ratio.

Fig. 14 shows the influence of the angle φ on the auto-correlation coefficient function of u-component. It is seen that the auto-correlation coefficient function decrease with the increasing angle φ. It indicates that the increasing of angle φ results in the decrease of length scale 'seen' from the moving vehicle, which is more significant with the increasing speed ratio.

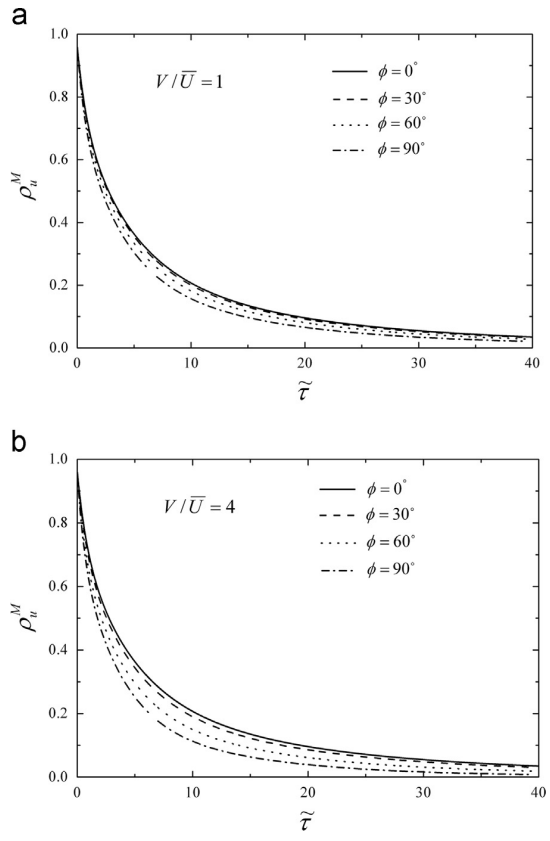

Fig. 14. The influence of angle φ on longitudinal auto-correlation coefficient function: (a) $V/\overline{U}=1$, (b) $V/\overline{U}=4$, (symbol: φ=vehicle moving direction; $V/\overline{U}$=speed ratio).

4.3. Cross-correlation coefficient function

Fig. 15 shows the cross-correlation coefficient function of u-component of wind fluctuation for different non-dimensional separation distance $\tilde{d} = (\eta' - \eta)/z$ and different speed ratios $V/\overline{U} = 1$ and 4, where $\zeta' = \zeta$. The wind direction is normal to the moving vehicle, i.e., $\varphi = 90^\circ$. With consideration of vehicle motion, it can be seen that the turbulence cross-correlation coefficient rise to a maximum value at some value of the time delay, which is a function of the separation distance and speed ratio.

4.4. Coherence function

The square-root coherence function is defined as follows:

$$\gamma_{ii}(\vec{r}, \vec{r'}; n) = \frac{\left|S_{ii}(\vec{r}, \vec{r'}; n)\right|}{S_i(n)} \tag{29}$$

where $S_{ii}(\vec{r}, \vec{r'}; n)$ is the single-sided cross-spectral density function; $S_i(n)$ is the power spectral density function of the i-component and $i = u$ or v. The cross-spectral density can be obtained from the cross-correlation function with the Fourier transformation.

Fig. 16 shows the coherence function of u-component for different separation distance $\Delta\eta$ and speed ratio $V/\overline{U}$ with $\varphi = 90^\circ$. The coherence function is plotted as a function of non-dimension frequency $\tilde{n} = n\Delta\eta/V_r$. It is noted that the coherence function increases with increasing speed ratio $V/\overline{U}$. That suggests that the wind fluctuations and thus the aerodynamic forces on moving vehicles are more correlated in space. Both the increases

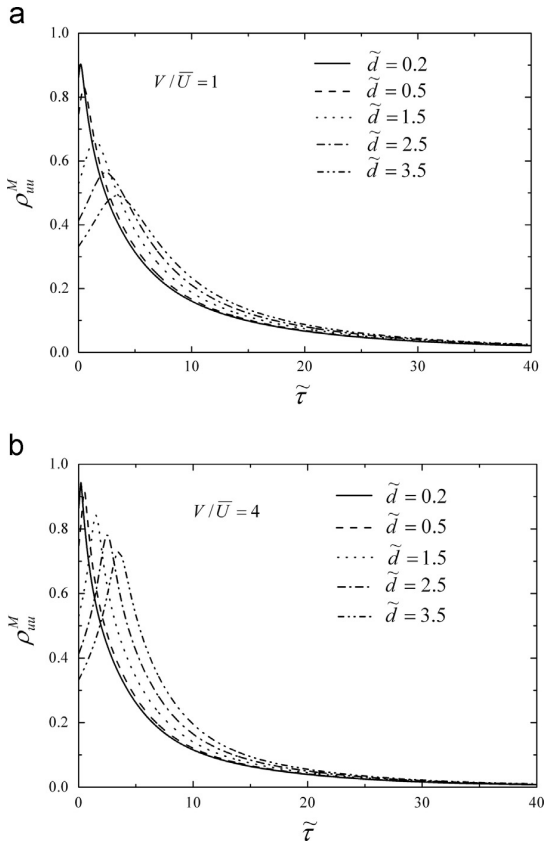

Fig. 15. Cross-correlation coefficient function relative to moving vehicles: (a) $V/\overline{U}=1$, (b) $V/\overline{U}=4$, (abscissa: $\tilde{\tau}$=non-dimensional time lag; ordinate: ρ_{uu}^M= cross-correlation coefficient function relative to moving vehicles; symbol: $\tilde{d}$=non-dimensional separation distance; $V/\overline{U}$=speed ratio).

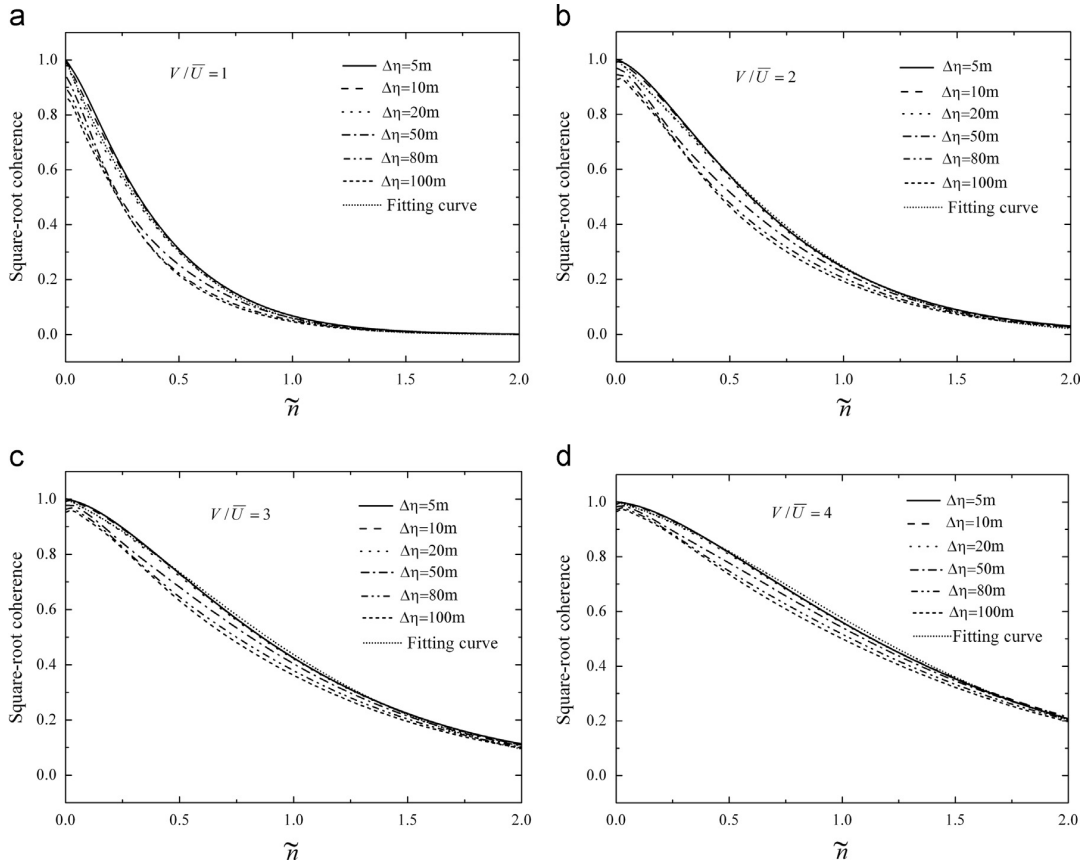

Fig. 16. The numerical curves and fitting curves of square-root coherence at different speed ratios: (a) $V/\overline{U}=1$, (b) $V/\overline{U}=2$, (c) $V/\overline{U}=3$, (d) $V/\overline{U}=4$, (abscissa: $\tilde{n}$=non-dimension frequency; symbol: $\Delta\eta$=separation distance; $V/\overline{U}$=speed ratio).

Table 1
The decay coefficient a at different speed ratios.

$V/\overline{U}$	1.0	2.0	3.0	4.0	5.0	>=6.0
a	2.00	0.77	0.38	0.22	0.14	0.10

Symbol: $V/\overline{U}$=speed ratio; a=decay coefficient in Eq. (30).

in coherence and the power spectrum contribute to larger aerodynamic forces and wind-induced vehicle vibration as the increasing speed ratio. It is also noted that the coherence function is less sensitive to the separation distance, especially when the speed ratio is high. Based on the calculated coherence function, the following approximate model can be developed by curve-fitting:

$$Coh(\tilde{n}) = \exp\left(-a\tilde{n}\sqrt{1+\left(\frac{V}{\overline{U}}\tilde{n}\right)^{1.2}}\right) \tag{30}$$

where a is the decay coefficient. The values of a at different speed ratios are listed in Table 1. It is obvious when $V=0$, the above coherence function model reduces to the traditional model widely used for coherence function of wind turbulence (Davenport, 1961).

5. Conclusions

This study presented derivations of auto-correlation coefficient function of lateral wind fluctuation and cross-correlation coefficient functions of lateral and longitudinal wind fluctuations from the Kaimal spectrum of longitudinal wind fluctuation on the basis of Taylor's frozen turbulence hypothesis and isotropic turbulence model. The power spectra and correlation coefficient functions of wind turbulence relative to moving vehicles were also deduced based on the same hypothesis. The results can be applied for any vehicle moving direction, and for both longitudinal and lateral components of wind turbulence. The results showed that, while the total energy of the turbulence was not affected, the moving vehicle experience higher wind energy at the frequency range of interest, thus leads to higher aerodynamic forces.

The motion of vehicle resulted in reducing the time of vehicle passing by the turbulent eddies, corresponding to the reduction of the average size of turbulent Eddies 'seen' from the moving vehicle. The coherence function increased with increasing speed ratio of moving vehicle to wind velocity. That suggested that the wind fluctuations and thus the aerodynamic forces on moving vehicles were more correlated in space. Both the increases in coherence and the power spectrum contributed to larger aerodynamic forces and wind-induced vehicle vibration as the increasing speed ratio.

Although the characteristic functions of lateral turbulence were derived from the power spectrum of longitudinal turbulence based on the isotropic turbulence assumption, these functions can also be determined from the spectrum of lateral turbulence when it is available.

Acknowledgments

The authors are grateful for the financial supports from the National Natural Science Foundation of China under Grant

NNSF-U1334201, 51278434, and the Fundamental Research Funds for the Central Universities (Project no. SWJTU11CX008). Sincere thanks also go to Huoyue Xiang and Ning Chen at the Southwest Jiaotong University for their encouraging comments.

References

Baker, C.J., 1991a. Ground vehicles in high cross winds Part I: steady aerodynamic forces. J. Fluids Struct. 5, 69–90.
Baker, C.J., 1991b. Ground vehicles in high cross winds Part II: unsteady aerodynamic forces. J. Fluids Struct. 5, 91–111.
Baker, C.J., 1991c. Ground vehicles in high cross winds Part III: The interaction of aerodynamic forces and the vehicle system. J. Fluids Struct 5, 221–241.
Baker, C.J., 2013. A framework for the consideration of the effects of crosswinds on trains. J. Wind Eng. Ind. Aerodyn. 123, 130–142.
Balzer, L.A., 1977. Atmospheric turbulence encountered by high-speed ground transport vehicles. J. Mech. Eng. Sci 19, 227–235.
Batchelor, G.K., 1953. Theory of Homogeneous Turbulence. Cambridge Univ. Press, Cambridge.
Cai, C.S., Chen, S.R., 2004. Framework of vehicle–bridge–wind dynamic analysis. J. Wind Eng. Ind. Aerodyn. 92, 579–607.
Cheli, F., Corradi, R., Tomasini, G., 2012. Crosswind action on rail vehicles: a methodology for the estimation of the characteristic wind curves. J. Wind Eng. Ind. Aerodyn. 104-106, 248–255.
Cooper, R.K., 1984. Atmospheric turbulence with respect to moving ground vehicles. J. Wind Eng. Ind. Aerodyn. 17, 215–238.
Davenport, A.G., 1961. The spectrum of horizontal gustiness near the ground in high winds. Q. J. R. Meteorol. Soc. 87, 194–211.
Diedrichs, B., 2006. Studies of two aerodynamics effects on high-speed trains crosswind stability and discomforting car body vibrations inside tunnels (Ph.D. thesis). Aeronautical and Vehicle Engineering. Royal Institute of Technology, Stockholm, Sweden.
ESDU, 1985. Characteristics of atmospheric turbulence near the ground. Part II: single point data for strong winds (neutral atmosphere). Item No. 85020, Engineering Sciences Data Unit, London.
ESDU. 1986. Characteristics of atmospheric turbulence near the ground. Part III: variations in space and time for strong winds (neutral atmosphere). Item No. 86010, Engineering Sciences Data Unit, London.
Gawthorpe, R.G., 1994. Wind effects on ground transportation. J. Wind Eng. Ind. Aerodyn. 52, 73–92.
Gifford, F., 1956. The relationship between space and time correlation in the atmosphere. J. Meteorol. 13, 289–294.
Gradsbteyn, I.S., Ryzbik, L.M., 2000. Table of Integrals, Series and Products, 6th Ed. Academic Press, New York.
Johnson, T., 1996. Strong wind effects on railway operations-16th October 1987. J. Wind Eng. Ind. Aerodyn. 60, 251–266.
Kaimal, J.C., Wyngaard, J.C., Izumi, Y., Cote, O.R., 1972. Spectral characteristics of surface-layer turbulence. Q. J. R. Meteorol. Soc. 98, 563–589.
Karman, Th. Von, 1937. The fundamentals of the statistical theory of turbulence. J. Aero. Sci. 4, 131–138.
Landahl, M.T., Christensen, E.M., 1992. Turbulence and Random Process in Fluid Mechanics, 2nd Ed. Cambridge University Press.
Lappe, U.O., Davidson, B., 1963. On the range of validity of Taylor's hypothesis and the Kolmogoroff spectral law. J. Atmos. Sci. 20, 569–576.
Li, Y.L., Qiang, S.Z., Liao, H.L., Xu, Y.L., 2005. Dynamics of wind-rail vehicle-bridge systems. J. Wind Eng. Ind. Aerodyn. 93, 483–507.
Lin, C.C., 1953. On Taylor's hypothesis and the acceleration terms in the Navier Stokes equations. Q. Appl. Math. 10, 295–306.
Liu, H.T., 2011. Dynamic responses of coupled train, automobile and bridge system under strong wind and analysis of running safety and riding comfort of vehicles (Ph.D. Thesis). Bridge and Tunnel Engineering. Central South University, Changsha, China (in Chinese),.
Taylor, G.I., 1938. The spectrum of turbulence (London). Proc. R. Soc. A164, 476–490.
Xu, Y.L., Guo, W.H., 2003. Dynamic analysis of coupled road vehicle and cable-stayed bridge systems under turbulent wind. Eng. Struct. 25, 473–486.